ORIGINAL RESEARCH

Doxorubicin and indocyanine green loaded superparamagnetic iron oxide nanoparticles with PEGylated phospholipid coating for magnetic resonance with fluorescence imaging and chemotherapy of glioma

Chen Shen[1,2,*]
Xiaoxiong Wang[1,2,*]
Zhixing Zheng[1,2,*]
Chuang Gao[3]
Xin Chen[1,2]
Shiguang Zhao[1,2]
Zhifei Dai[3]

[1]Department of Neurosurgery, First Affiliated Hospital of Harbin Medical University, Harbin, Heilongjiang, China; [2]Institute of Neuroscience, Sino-Russian Medical Research Center, Harbin Medical University, Harbin, Heilongjiang, China; [3]Department of Biomedical Engineering, College of Engineering, Peking University, Beijing, China

*These authors contributed equally to this work

Correspondence: Shiguang Zhao
Department of Neurosurgery, First Affiliated Hospital of Harbin Medical University, No 23 Youzheng Street, Nangang District, Harbin, Heilongjiang 150001, China
Tel +86 451 8555 2799
Fax +86 451 5362 9254
Email guangsz@hotmail.com

Zhifei Dai
Department of Biomedical Engineering, College of Engineering, Peking University, No 5 Yiheyuan Road, Haidian District, Beijing 100871, China
Tel +86 152 1016 8242
Email zhifei.dai@pku.edu.cn

Background: Glioma represents the most common malignant brain tumor. Outcomes of surgical resection are often unsatisfactory due to low sensitivity or resolution of imaging methods. Moreover, the use of traditional chemotherapeutics, such as doxorubicin (DOX), is limited due to their low blood–brain barrier (BBB) permeability. Recently, the development of nanotechnology could overcome these obstacles.

Materials and methods: Hydrophobic superparamagnetic iron oxide nanoparticles (SPIO NPs) were prepared with the use of thermal decomposition method. They were coated with 1,2-distearoyl-sn-glycero-3-phosphoethanolamine-*N*-[methoxy(polyethylene glycol)-2000] (DSPE-PEG 2000) and DOX using a thin-film hydration method followed by loading of indocyanine green (ICG) into the phospholipid layers. Details regarding the characteristics of NPs were determined. The in vitro biocompatibility and antitumor efficacy were established with the use of MTT assay. In vivo fluorescence and magnetic resonance (MR) imaging were used to evaluate BBB penetration and accumulation of NPs at the tumor site. Antitumor efficacy was evaluated using measures of tumor size, median survival times, body weights, and H&E staining.

Results: The multifunctional NPs generated had an average diameter of 22.9 nm, a zeta potential of −38.19 mV, and were capable of providing a sustained release of DOX. In vitro experiments demonstrated that the SPIO@DSPE-PEG/DOX/ICG NPs effectively enhanced cellular uptake of DOX as compared with that of free DOX. In vivo fluorescence and MR imaging revealed that the NPs not only effectively crossed the BBB but selectively accumulated at the tumor site. Meanwhile, among all groups studied, C6 glioma-bearing rats treated with the NPs exhibited the maximal degree of therapeutic efficacy, including smallest tumor volume, lowest body weight loss, and longest survival times, with no obvious side effects.

Conclusion: These results suggest that the SPIO@DSPE-PEG/DOX/ICG NPs can not only function as a nanoprobe for MR and fluorescence bimodal imaging, but also as a vehicle to deliver chemotherapeutic drugs to the tumor site, to achieve the theranostic treatment of glioma.

Keywords: SPIO NPs, BBB, MR imaging, fluorescence imaging, chemotherapy

Introduction

Glioblastoma multiforme (GBM), which is a type of neuroepithelial tumor, represents the most commonly occurring primary central nervous system tumor in adults.[1] With its characteristic of excessive invasiveness, GBM is infamous for its invariable

recurrence, high mortality rate, and limited survival time.[2,3] Currently, the standard treatment for GBM involves a multimodality approach consisting of surgical resection, whenever possible, combined with chemotherapy and radiotherapy. Unfortunately, the therapeutic efficacy and prognosis for this condition is far from satisfactory.[4,5]

Currently, an increasing number of auxiliary techniques have been applied during surgery, such as intraoperative magnetic resonance imaging (iMRI) and fluorescence-guided surgery, to improve the safety of these surgeries and to increase the resection rate.[6,7] However, the outcomes of many of these techniques are often unsatisfactory due to either low sensitivity or poor resolution.[8,9] Combining techniques also has its liabilities as this requires multiple injections of contrast agents, which can result in additional trauma and increases the patient's metabolic burden. In addition, the presence of the blood–brain barrier (BBB) severely limits the delivery of most therapeutic agents, such as doxorubicin (DOX), to brain tissue.[10] The few chemotherapeutic drugs capable of transporting through the BBB are usually incapable of effectively locating the tumor site to achieve the necessary concentrations required to destroy tumor cells without damaging normal brain tissue or other organs.[11]

Recently, the development of NPs has generated a promising new approach for the treatment of glioma.[12,13] However, biocompatibility of the nanocarriers remains a primary factor that hinders their clinical application.[14] The first NPs to be used clinically as an MRI T_2 contrast agent involved superparamagnetic iron oxide NPs (SPIO NPs), which exhibited excellent biocompatibility and imaging capacity.[15] The surfaces of SPIO NPs can be easily modified with surfactants and bioactive ligands, which further enhance their effectiveness by: 1) prolonging their circulatory duration, 2) enabling them to actively target specific sites, and 3) enabling NPs to be loaded with a broad range of diagnostic and therapeutic agents for the theranostic treatment of tumors.[16,17] Although MRI has excellent spatial resolution, it is limited by its poor sensitivity.[8] In contrast, near-infrared (NIR) fluorescence imaging, which has high sensitivity, exhibits relatively poor resolution.[9] Indocyanine green (ICG) is an amphiphilic tricarbocyanine dye exhibiting maximal absorption and emission in the NIR region around 780 and 810 nm, respectively.[18] It is the only NIR organic dye approved by the US Food and Drug Administration (FDA) for clinical applications and represents an agent with one of the lowest known toxicities in humans.[19,20] Currently, ICG is widely employed in ophthalmic angiography,[21]

cardiac output measurements,[22] and hepatic function assessments.[23] It is also widely used in neurosurgery for complex aneurysms,[24] arterio-venous malformations,[25] and arterio-venous fistulas.[26] It has been reported that ICG-loaded SPIO NPs could enhance photoacoustic tomography of brain vasculature and tumor.[27] In addition, nanocarriers have the capacity to deliver a number of chemotherapy drugs and imaging contrast agents to the tumor site.[28] Thus, an optimal approach would involve the construction of a multifunctional NP which integrates bimodal imaging and chemotherapy, so as to achieve the theranostic treatment of glioma.

In this study, we constructed a novel multifunctional drug delivery system. This system integrates real-time MR imaging, fluorescence imaging, and chemotherapy capabilities for the theranostic treatment of glioma. Construction of NPs consisted of coating hydrophobic SPIO NPs with 1,2-distearoyl-sn-glycero-3-phosphoethanolamine-*N*-[methoxy(polyethylene glycol)-2000] (DSPE-PEG 2000) and hydrophobic DOX through a thin-film hydration method followed by loading ICG into the lipid shell layers around the surface of the NPs (Figure 1). SPIO NPs were used for real-time MRI imaging and served as the core for the NPs, while lipid shell layers surrounding SPIO NPs served to carry DOX and ICG. ICG was used as an NIR fluorescence probe for real-time fluorescence imaging. We characterized the physicochemical properties of the NPs including morphology, particle size, zeta potential, and drug loading ability. Cellular uptake, biocompatibility, and cytotoxicity were assessed in vitro, while BBB transport and tumor imaging were investigated in an orthotopic glioma model using in vivo fluorescence and MR imaging. Finally, the antitumor efficacy, biocompatibility, and side effects of the DOX-loaded multifunctional NPs were carefully evaluated by assessing tumor size, body weight changes, median survival time, and results from H&E staining.

Materials and methods
Materials
Iron tri(acetyl acetonate), oleylamine, and oleic acid were purchased from J&K Chemical Ltd. (Beijing, China). DSPE-PEG 2000 was purchased from Advanced Viecle Technology Co., Ltd. (Shanghai, China). Doxorubicin hydrochloride (DOX.HCl) was purchased from Meilune Biological Technology Co., Ltd. (Dalian, China). MTT was purchased from Sigma-Aldrich Co. (Shanghai, China). DMEM and FBS were purchased from Thermo Fisher Scientific (Waltham,
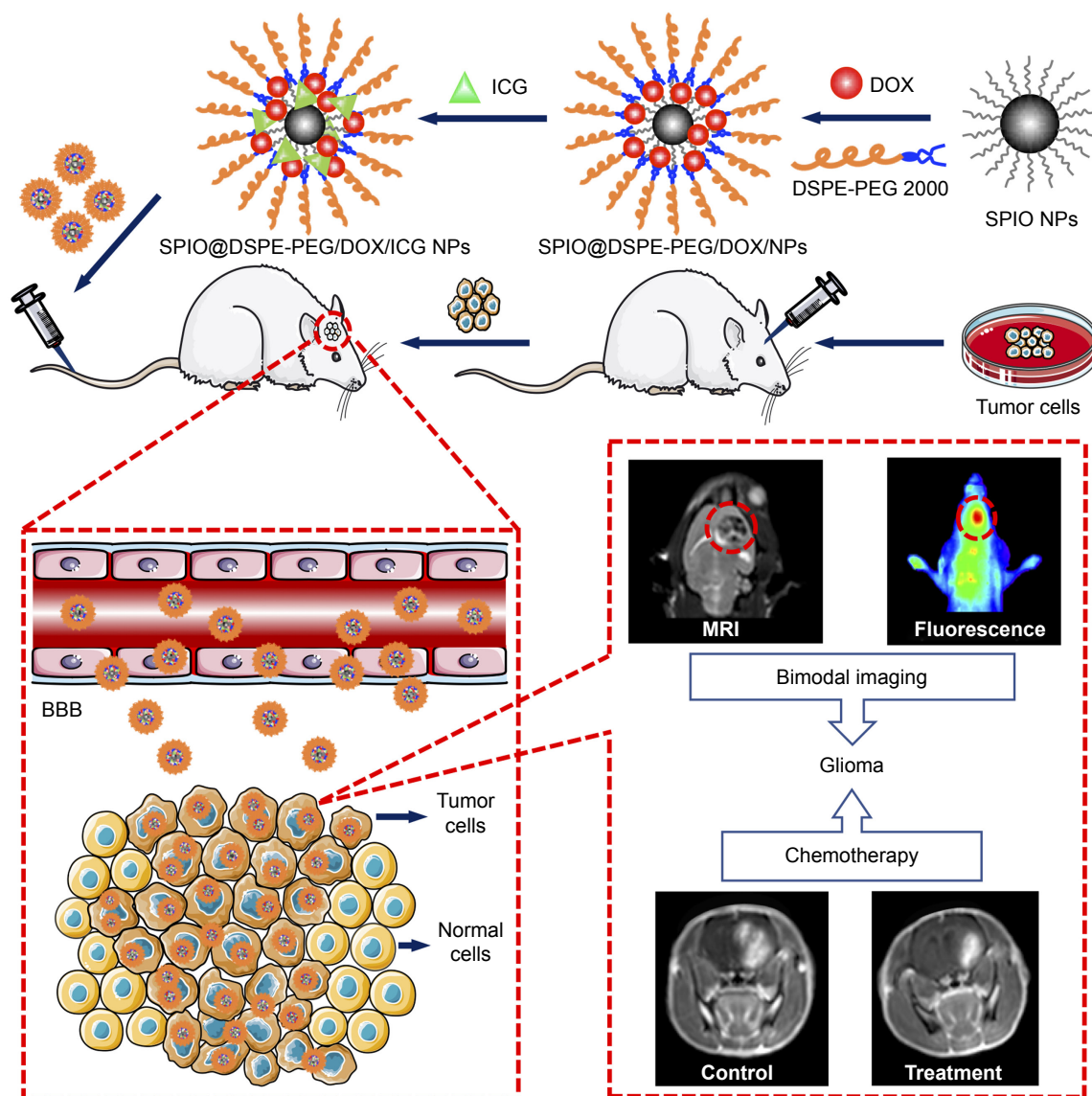
Figure 1 Schematic illustration. SPIO@DSPE-PEG/DOX/ICG NPs preparation procedure and MR/NIR fluorescence dual-modal imaging and chemotherapy of glioma through intravenous injection.

Abbreviations: BBB, blood–brain barrier; DOX, doxorubicin; DSPE-PEG, 1,2-distearoyl-sn-glycero-3-phosphoethanolamine-*N*-[methoxy(polyethylene glycol)]; ICG, indocyanine green; MR, magnetic resonance; SPIO NPs, superparamagnetic iron oxide nanoparticles; NIR, near-infrared.

MA, USA). Trypsin-EDTA (0.25%), streptomycin, and penicillin were purchased from Thermo Fisher Scientific.

Synthesis of SPIO NPs

The SPIO NP cores were prepared using the thermal decomposition method according to a previous report.[29] Briefly, iron tri(acetyl acetonate) 1.40 g, oleic acid 8.90 g, and oleylamine 8.13 g were mixed in a 100 mL three-neck flask. The mixture was heated from room temperature to 120°C for 30 minutes under nitrogen flow and maintained for 2 hours, then heated further to 220°C for 30 minutes and maintained

for 30 minutes. Finally, the temperature was increased to 300°C for 1 hour and maintained for 30 minutes. After being cooled to room temperature, the reaction mixture was washed three times with ethanol. After the final wash, the deposit was dissolved in toluene and the solution was stored at 4°C.

Preparation of drug-loaded NPs

The hydrophobic DOX was acquired according to a previous study.[30] The water-soluble drug-loaded SPIO@DSPE-PEG/DOX NPs were prepared using a thin-film hydration method. SPIO NPs 2 mg (iron content), hydrophobic DOX

1.5 mg, and DSPE-PEG 2000 4 mg were dissolved in chloroform. The solvent was removed with use of a rotary evaporator under vacuum and a thin lipid film formed on the wall of the flask. Ultrapure water was then added to the flask and hydrated for 30–60 minutes at 55–65°C. After water bath ultrasonication for 2 hours, the un-encapsulated hydrophobic DOX was removed by centrifugation at 1,500 rpm for 10 minutes. The empty micelles were removed by ultracentrifugation at $100,000\times g$. The DOX loading capacity (LC) and encapsulation efficiency (EE) were calculated according to the following formulae:

$$LC = \frac{\text{Mass of encapsulated DOX}}{\text{Mass of nanoparticles}} \times 100\%$$

$$EE = \frac{\text{Mass of encapsulated DOX}}{\text{Total mass of added DOX}} \times 100\%$$

Loading ICG into SPIO@DSPE-PEG/DOX NPs

ICG was loaded into SPIO@DSPE-PEG/DOX NPs as previously described.[31] Briefly, ICG (0.2 mg) was mixed with 1 mg (iron content) SPIO@DSPE-PEG/DOX NPs in a water solution. The mixture was stirred overnight at room temperature. Unloaded ICG molecules were removed using an ultrafiltration centrifugation device with a polyethersulfone membrane (100 kDa cutoff size).

Characterization of nanoparticles

Fluorescence spectra were collected by a fluorescence spectrophotometer (Varian Cary Eclipse; Varian Inc., Palo Alto, CA, USA). Particle morphological examination was performed using transmission electron microscopy (TEM, Hitachi H-7650; Hitachi, Tokyo, Japan). Hydrodynamic diameters and zeta potentials of NPs were determined by 90Plus/BI-MAS dynamic light scattering (DLS) analyzer (ZetaPALS; Brookhaven Instruments Corporation, Holtsville, NY, USA) at room temperature. The iron concentration was measured using an Optima 5,300 DV inductively coupled plasma optical emission spectrometer (Perkin-Elmer, Waltham, MA, USA).

In vitro drug release

The release characteristics of DOX were investigated in pH 7.4 PBS at 37°C. Two milliliters of dispersed DOX-loaded NPs were sealed in a dialysis bag (molecular weight cutoff 14,000 Da; Viskase companies, Inc., Chicago, IL, USA), immersed in 50 mL of PBS preheated to 37°C

and subjected to continuous shaking. Samples (2 mL) were removed at predetermined time intervals and replaced with 2 mL of PBS. The amount of DOX released from NPs was then determined by using a fluorescence spectrophotometer and compared with values generated from a standard curve. The excitation and emission wavelengths were 480 and 590 nm, respectively. All experiments were carried out in triplicate.

In vitro cellular uptake

U251 cells (purchased from iCell Bioscience Inc, Shanghai, China) were grown on cover slips in six-well plates at a density of 1×10^6 cells per well and were allowed to adhere for 24 hours. The medium was then removed and cells were incubated with fresh medium containing free DOX or SPIO@DSPE-PEG/DOX/ICG NPs (6 µg/mL equivalent DOX). After incubating for 1 hour, cells were washed with PBS, fixed with 4% paraformaldehyde, and qualitatively analyzed with confocal laser scan microscopy (CLSM, Olympus FV300; Olympus, Tokyo, Japan). The fluorescence pictures were captured using the following parameters: photomultiplier tube =545 v; gain =5.0 x; offset =10%; laser intensity: red =50.0, blue =20.0; Scan size =1,024×1,024.

Biocompatibility evaluation and cytotoxicity analysis

The biocompatibility and cytotoxicity in vitro were evaluated using an MTT assay. To evaluate the biocompatibility of blank SPIO@DSPE-PEG NPs, human umbilical vein endothelial cells (HUVECs; iCell Bioscience Inc) were uniformly seeded in a 96-well plate with a density of 5×10^3 cells per well in H-DMEM medium supplemented with FBS (10%) and incubated for 24 hours at 37°C. Varying concentrations of blank NPs (equivalent to Fe concentrations) were then added to the cells and incubated for another 24, 48, or 72 hours, at which time the medium was discarded. The MTT stock solution (20 µL, 5 mg/mL) was then added to each group and incubation was continued for another 4 hours. Finally, supernatants were totally replaced with 200 µL of dimethyl sulfoxide. Absorbance was measured at 490 nm using a microplate reader (BioTek ELx800; Bio Tek, Winooski, VT, USA).

To investigate the antitumor efficacy of SPIO@DSPE-PEG/DOX/ICG NPs in vitro, 5×10^3 U251 cells were seeded in 96-well plates and incubated for 24 hours. Following attachment, the cells were exposed to varying concentrations of free DOX or NPs for 24, 48, or 72 hours. Cell viability was then determined by using the MTT assay as described above.

Animal model

BALB/c nude mice and Wistar rats, purchased from Vital River Laboratory Animal Technology Co., Ltd. (Beijing, China), were used to establish an orthotopic glioma model. BALB/c nude mice (female, 18–22 g) were housed under specific pathogen-free conditions. After anesthetization with 10% chloralic hydras (3 mL/kg, intraperitoneal [ip]), animals were immobilized in a stereotactic fixation device. For implantation of C6 glioma cells (iCell Bioscience Inc), a sagittal incision was made through the skin overlying the calvarium, and a small dental drill was used to create a hole (1.0 mm diameter) in the cranium 1.0 mm anterior to bregma and 2 mm lateral to the right sagittal suture without dura-matral damage. Subsequently, ~1×10^5 of the C6 glioma cell suspension in 5 µL (suspended by PBS) was slowly injected at a depth of 3 mm from the skull base. The incision was sutured using silk braid and a medical suture needle.

Wistar rats (female, 140–160 g) were stereotaxically inoculated with 2×10^6 C6 cells (in 10 µL PBS) into the right hemisphere of the brain (1 mm anterior to bregma and 3 mm lateral to the sagittal suture, at a depth of 5 mm from the skull base). All animal experiments conducted in this study were evaluated and approved by the Animal Care and Ethical Committee of the First Affiliated Hospital of Harbin Medical University and conducted based on state guidelines from the Ministry of Science and Technology of China.

Tumor fluorescence imaging in vivo

For investigating tumor fluorescence imaging capability and visualizing in vivo real-time distribution of the NPs, SPIO@DSPE-PEG/DOX/ICG NPs and free ICG were injected in tumor-bearing BALB/c nude mice through the tail vein at 18 days after implantation. Fluorescence images were taken with use of an IVIS spectrum imaging system (PerkinElmer) after injection at different time points. A filter set (E_x=745 nm, E_m=840 nm) was used for the measurement of ICG. During the imaging process, the mice were maintained on the imaging stage under anesthetization with 2.5% isoflurane gas in oxygen flow. After imaging, tumor-bearing mice were euthanized and main organs were removed for determining the distribution of NPs in vivo.

Tumor MR imaging in vivo

Eighteen days after implantation, in vivo MR imaging was performed using a 3.0 T Achieva MR System (Philips Healthcare, the Netherlands) with a four-channel mouse head coil. Tumor-bearing Wistar rats were imaged using a spin-echo sequence (repetition time =3,000 ms; echo time =80 ms; number of excitation =3; matrix size =256×256; field of view =43 mm; slice thickness =1 mm; slice spacing =1.2 mm). Animals were anesthetized with 10% chloralic hydras (3 mL/kg; .p) for 10 minutes prior to the MRI procedure. Images were taken before and after the tail vein injection of SPIO@DSPE-PEG/DOX/ICG NPs (10 mg Fe/kg) at different time points.

In vivo antitumor efficacy

Thirty-eight glioma-bearing Wistar rats were randomly divided into four groups according to their MR images and treated with saline, SPIO@DSPE-PEG NPs, free DOX or SPIO@DSPE-PEG/DOX/ICG NPs (at an equal dose of 5 mg/kg DOX). All groups were treated on days 7, 14, 21, and 28 after C6 glioma cell inoculation. Following these treatments, all but six rats from each group were euthanized for collection of major organs. The obtained brains were frozen and stained with TUNEL to observe cell apoptosis in the glioma tissues. The cell nucleus was stained with DAPI and examined with use of a fluorescent microscope (Olympus). The remaining six rats from each group were monitored for treatment efficacy. Efficacy of the NPs was further evaluated by MR imaging of glioma size and measuring body weights and survival times following treatments.

Histology analysis

Major organs were immediately fixed in 4% paraformaldehyde, embedded in paraffin, and sliced into 5-µm-thick sections which were stained with H&E for histological examination. Organ histology was viewed and imaged under light microscopy (Nikon E800; Jiangsu JEDA SmartV350D Imaging System).

Statistical analysis

Data are presented as mean ± SD. One-way ANOVA was used for a multiple-group analysis and Student's t-tests were used for the two-group comparison. $P<0.05$ was considered statistically significant.

Results
Preparation and characterization of nanoparticles

The hydrophobic SPIO NPs stabilized with oleylamine and oleic acid were prepared with use of the thermal decomposition method. The diameter and zeta potentials of SPIO NPs were 9.8±0.09 nm and −38.63±0.1 mV, respectively (Table 1). The DOX-loaded NPs were coated with DSPE-PEG 2000 using a classic thin-film hydration method. The diameter and zeta potentials of SPIO@DSPE-PEG/DOX

Table 1 Physicochemical properties of nanoparticles

Nanoparticles	Hydrophobic SPIO NPs	SPIO@DSPE-PEG/DOX NPs	SPIO@DSPE-PEG/DOX/ICG NPs
Size d (nm)	9.8±0.09	20.6±2.10	22.9±1.80
Zeta potential (mV)	−38.63±0.10	−38.52±0.12	−38.19±0.06
DOX LC (%)	–	14.45±0.55	13.87±0.52
DOX EE (%)	–	67.45±2.82	67.45±2.82
ICG LC (%)	–	–	4.86±0.14
ICG EE (%)	–	–	73.48±2.44

Note: Data are represented as mean ± SD (n=3).
Abbreviations: DOX, doxorubicin; DSPE-PEG, 1,2-distearoyl-sn-glycero-3-phosphoethanolamine-*N*-[methoxy(polyethylene glycol)]; EE, encapsulation efficiency; ICG, indocyanine green; LC, loading capacity; SPIO NPs, superparamagnetic iron oxide nanoparticles.

NPs increased to 20.6±2.1 nm and −38.52±0.12 mV, respectively. The DOX LC and EE were 14.45% and 67.57%, respectively. ICG molecules could be easily loaded into the phospholipid layer of the NPs due to the amphiphilic nature of their structure. The diameter, zeta potentials, and DOX LC of SPIO@DSPE-PEG/DOX/ICG NPs changed to 22.9±1.8 nm, −38.19±0.06 mV, and 13.87% post-loading

of ICG, respectively. The ICG LC and EE were 4.86% and 73.48%, respectively.

The NPs obtained were further examined with TEM (Figure 2A and C). The coating layer was visible in TEM images with negative staining. The NPs exhibited a spherical shape or sphere-like morphology with an obvious core−shell structure. These results suggested that there was no significant
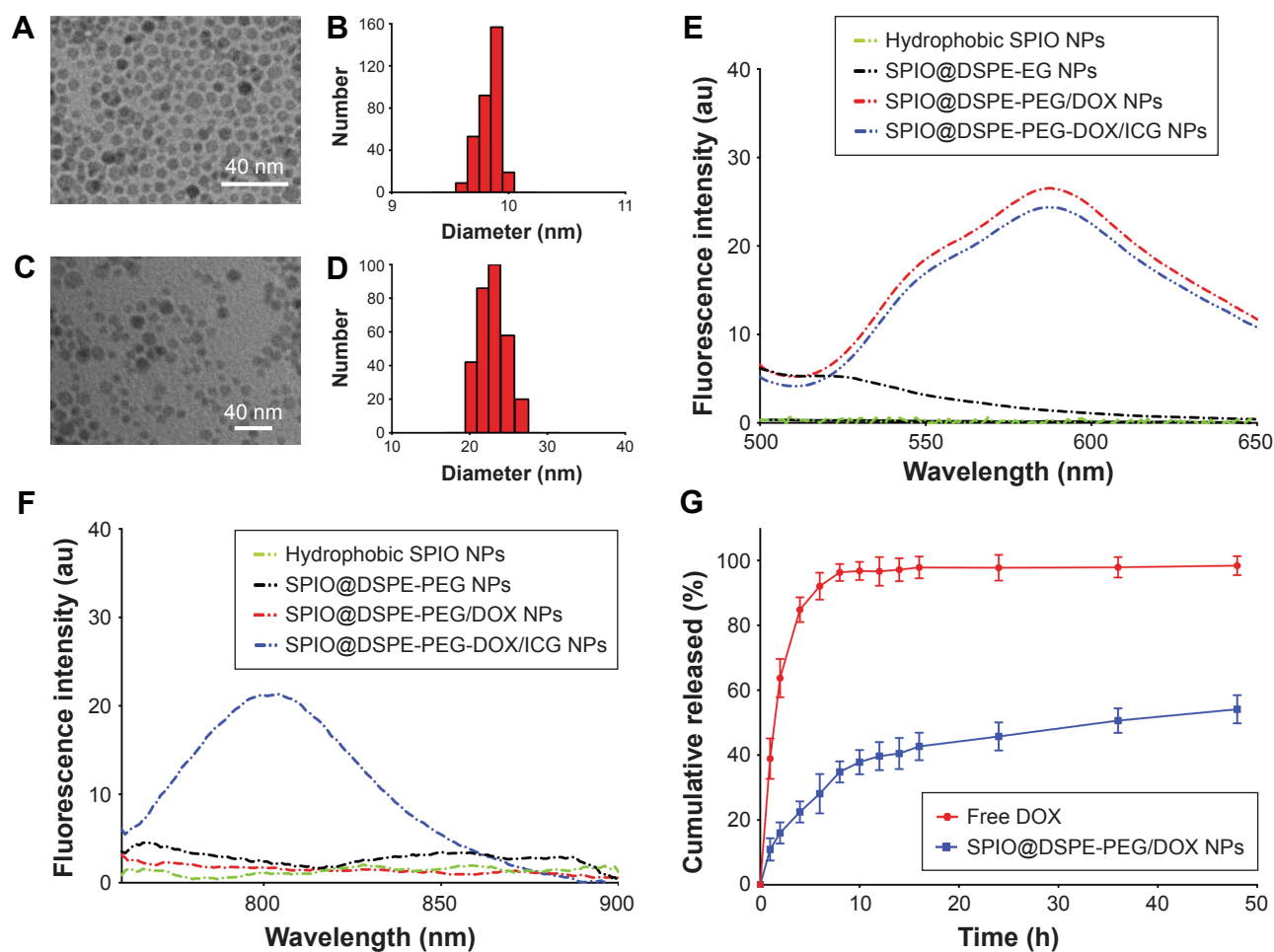

Figure 2 Characterization of nanoparticles.
Notes: TEM images of hydrophobic SPIO NPs (**A**) and SPIO@DSPE-PEG/DOX/ICG NPs (**C**). The bar represents 40 nm. Particle size distribution of hydrophobic SPIO NPs (**B**) and SPIO@DSPE-PEG/DOX/ICG NPs (**D**) by DLS measurements. Fluorescence spectra of nanoparticles with an excitation wavelength of 480 nm (**E**) and 740 nm (**F**). In vitro release profiles of DOX in PBS at 37°C (**G**). Data are presented as mean ± SD, n=3.
Abbreviations: DLS, dynamic light scattering; DOX, doxorubicin; DSPE-PEG, 1,2-distearoyl-sn-glycero-3-phosphoethanolamine-*N*-[methoxy(polyethylene glycol)]; ICG, indocyanine green; SPIO NPs, superparamagnetic iron oxide nanoparticles; TEM, transmission electron microscopy.

change in NP morphology after DOX or ICG loading. The NP size, as measured using TEM, was consistent with the hydrodynamic diameter evaluated using DLS (Figure 2B and D).

The fluorescence spectra of NPs are shown in Figure 2E and F. The SPIO@DSPE-PEG/DOX NPs and SPIO@DSPE-PEG/DOX/ICG NPs exhibited a broad absorbance peak between 550 and 650 nm with an excitation wavelength of 480 nm, while the hydrophobic SPIO NPs and SPIO@DSPE-PEG NPs exhibited no absorbance peak (Figure 2E). The SPIO@DSPE-PEG/DOX/ICG NPs exhibited a broad absorbance peak between 760 and 850 nm with an excitation wavelength of 740 nm, while the other three NPs exhibited no absorbance peak (Figure 2F). These findings indicated that DOX and ICG were successfully loaded into the NPs.

The release profiles of DOX from NPs were evaluated in PBS (pH 7.4) with free DOX being used as a control. As shown in Figure 2G, free DOX exhibited an initial surge in release with over 90% of DOX being released within 6 hours. In contrast, the DOX within NPs exhibited a biphasic release pattern comprised of a relatively fast initial release surge followed by a sustained release profile. About 37% of the DOX from these NPs was released during first 10 hours, and about 54% over the 48-hour period.

Cellular uptake of nanoparticles

In vitro cellular uptake was determined as a means to establish whether SPIO@DSPE-PEG NPs, as a carrier for DOX, could be taken up by U251 glioma cells. After incubation with either free DOX or DOX-loaded NPs (at equivalent DOX concentrations) for 1 hour at 37°C, the fluorescence intensity and distribution of DOX in U251 cells were observed with use of CLSM. As shown in Figure 3, tumor cells treated with free DOX showed DOX fluorescence limited to the cell nucleus, while DOX fluorescence was present in both the karyon and cytoplasm in equal concentrations with SPIO@DSPE-PEG/DOX/ICG NPs. In addition, the fluorescence intensity of the nucleus in the NPs group was stronger than that of the free DOX group.

Cytotoxicity of nanoparticles

In order to sufficiently study the potential for SPIO@DSPE-PEG NPs to serve as a drug carrier, the cytotoxicity of blank NPs upon HUVECs was firstly evaluated with use of the MTT assay. The viability of HUVECs after incubation with SPIO@DSPE-PEG NPs at varying concentrations (equivalent to Fe concentrations) for 24, 48, or 72 hours is shown in Figure 4A. There were no significant differences in cell survival rates at different concentrations and time points tested. Remarkably, cell viability remained at over 90%, even with a 72-hour incubation period using concentrations up to 100 μg/mL of Fe. Therefore, blank SPIO@DSPE-PEG NPs exhibited no obvious cytotoxicity and exhibited excellent biocompatibility for cells.

To investigate the in vitro antitumor efficacy of the multifunctional NPs, glioma U251 cells were incubated
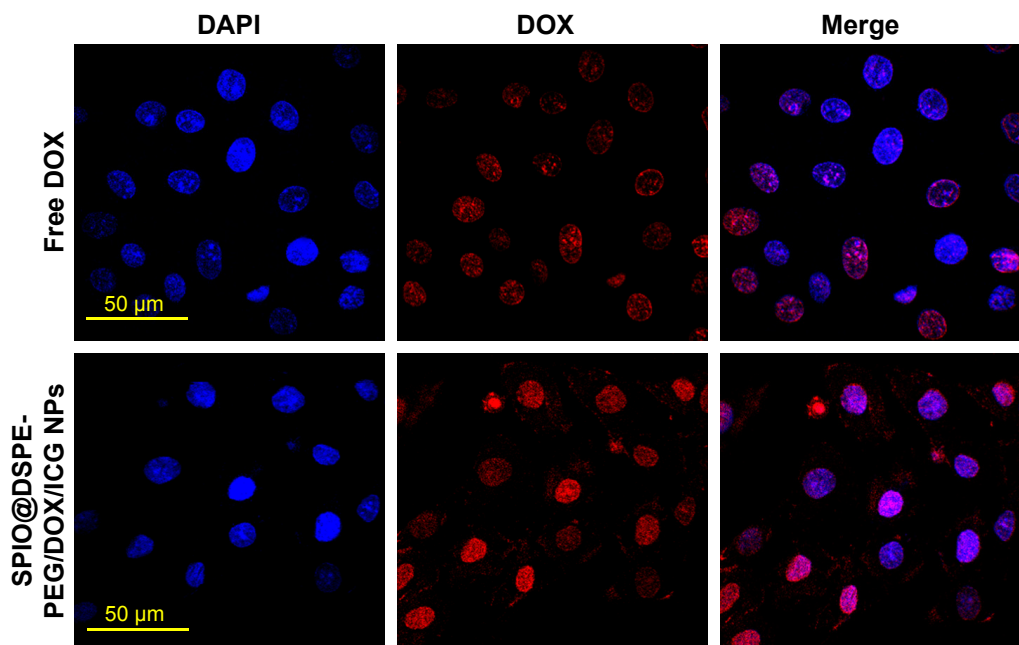
Figure 3 Cellular uptake of nanoparticles.
Note: CLSM images of U251 cells incubated with free DOX and SPIO@DSPE-PEG/DOX/ICG NPs at a DOX concentration of 6 μg/mL for 1 hour.
Abbreviations: CLSM, confocal laser scan microscopy; DOX, doxorubicin; DSPE-PEG, 1,2-distearoyl-sn-glycero-3-phosphoethanolamine-*N*-[methoxy(polyethylene glycol)]; ICG, indocyanine green; SPIO NPs, superparamagnetic iron oxide nanoparticles.
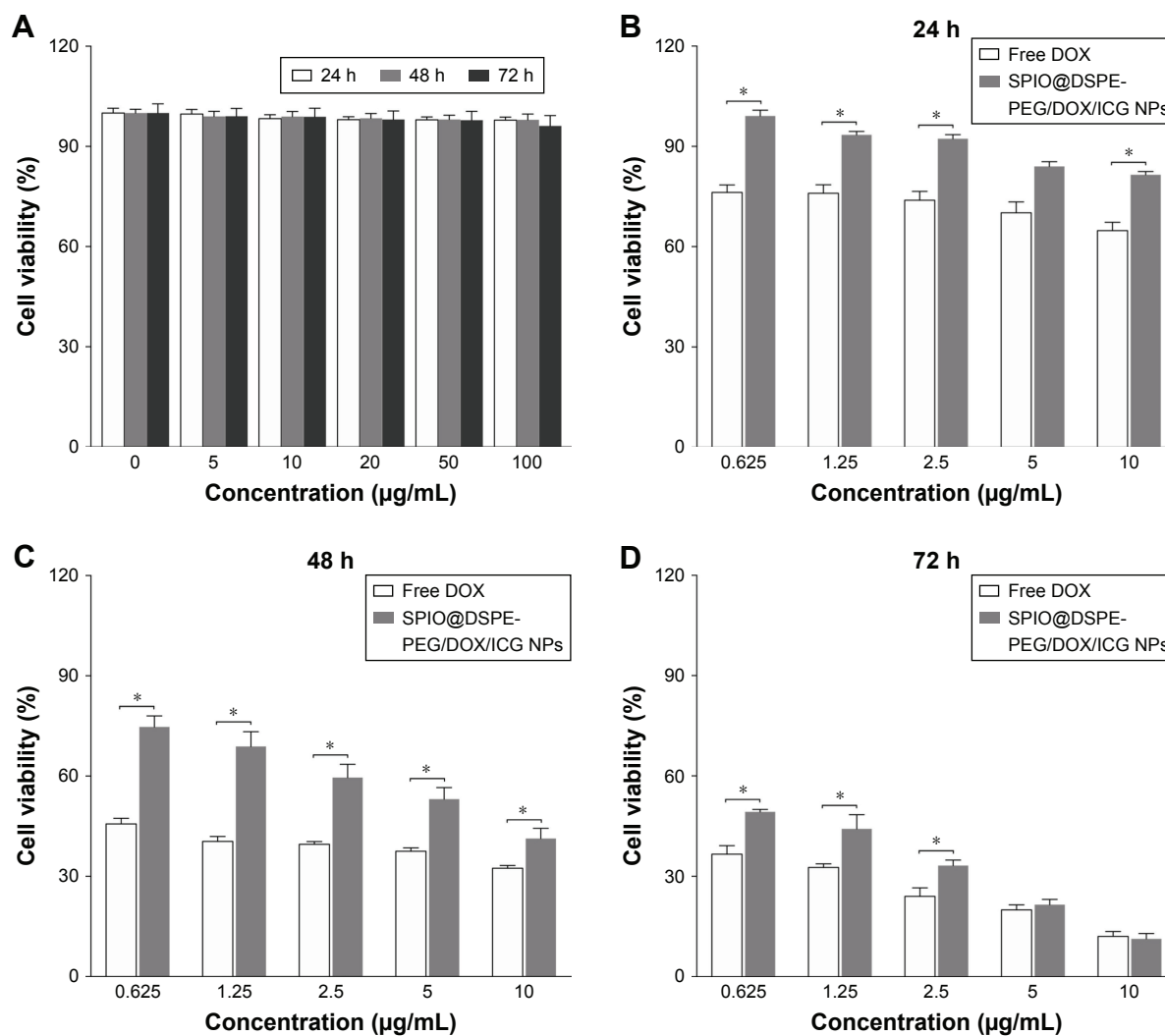
Figure 4 Biocompatibility and cytotoxicity of nanoparticles in vitro.
Notes: Viability of HUVEC cells after incubation with blank SPIO@DSPE-PEG NPs at varying concentrations (equivalent to Fe concentrations) for 24, 48, and 72 hours (**A**). In vitro antitumor efficiency of SPIO@DSPE-PEG/DOX/ICG NPs or free DOX (control) against U251 cells at different concentrations for 24 hours (**B**), 48 hours (**C**), and 72 hours (**D**). Data are mean ± SD, n=3, *$P<0.05$ vs free DOX group.
Abbreviations: DOX, doxorubicin; DSPE-PEG, 1,2-distearoyl-sn-glycero-3-phosphoethanolamine-*N*-[methoxy(polyethylene glycol)]; HUVEC, human umbilical vein endothelial cells; ICG, indocyanine green; SPIO NPs, superparamagnetic iron oxide nanoparticles.

with either SPIO@DSPE-PEG/DOX/ICG NPs or free DOX (control) at different concentrations for 24, 48, or 72 hours and cell viability was monitored with use of the MTT assay. As shown in Figure 4B–D, viability of U251 cells for all groups was dose- and time-dependent. As drug concentrations and incubation times increased, cell viability decreased, suggesting increased degrees of cytotoxicity. Viability of tumor cells treated with SPIO@DSPE-PEG/DOX/ICG NPs was found to be higher than that of free DOX after 24 and 48 hours of incubation periods (Figure 4B and C). However, after a 72-hour incubation period, the NPs exhibited enhanced cytotoxicity of cancer cells relative to that obtained at 24 and 48 hours of incubation and similar levels of cytotoxicity to those observed for free DOX at concentrations of 5 and 10 μg/mL (Figure 4D).

Tumor fluorescence imaging and tissue distribution in vivo

An in vivo near-infrared fluorescence imaging approach was utilized to monitor glioma targeting and fluorescence imaging efficiency of the multifunctional NPs in glioma-bearing mice. On the 18th day after implantation, mice were injected with free ICG and SPIO@DSPE-PEG/DOX/ICG NPs via the tail vein. The fluorescence intensity and signal distribution changes as determined at different times after administration are shown in Figure 5A. The fluorescence signals of free ICG were observed throughout the body at 2 hours post-injection, followed by a gradual time-dependent weakening of the signal and an absence of intense signals localized to the tumor site. By contrast, for the NPs group, after an initial period of dispersed signal locations, the presence of
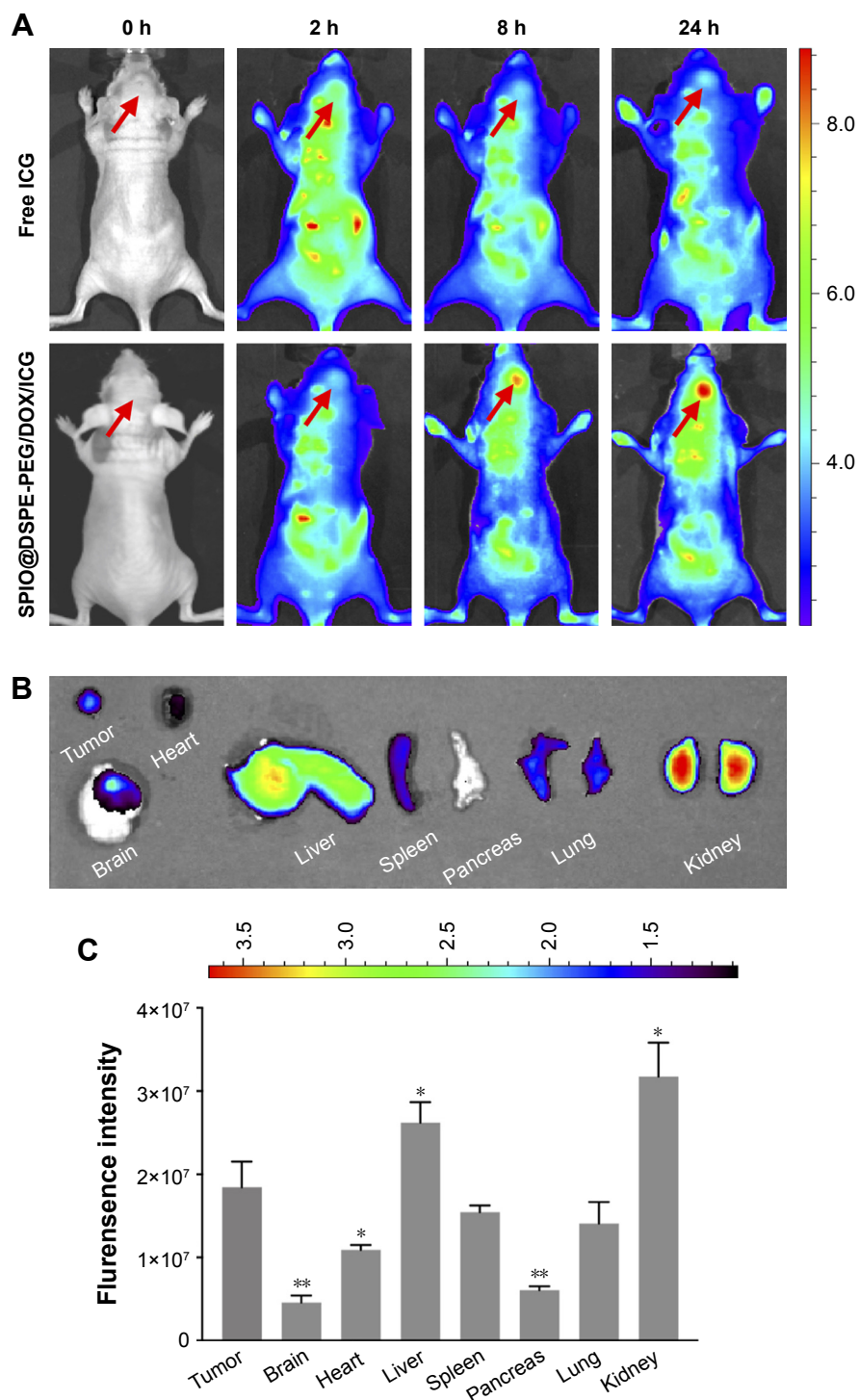
Figure 5 In vivo fluorescence imaging efficacy.
Notes: Fluorescence images of glioma-bearing nude mice at different times after tail vein injection of free ICG and SPIO@DSPE-PEG/DOX/ICG NPs (**A**); arrow indicates direction of the glioma. Ex vivo fluorescence images (**B**) and quantitative analysis (**C**) of main organs from glioma-bearing nude mice after 72 hours of tail vein injection. Data are mean ± SD, n=3, *$P<0.05$, **$P<0.01$ vs flurensence intensity in tumor.
Abbreviations: DOX, doxorubicin; DSPE-PEG, 1,2-distearoyl-sn-glycero-3-phosphoethanolamine-*N*-[methoxy(polyethylene glycol)]; ICG, indocyanine green; SPIO NPs, superparamagnetic iron oxide nanoparticles.

fluorescence signals was observed to be heightened in the tumor. At 24 hours, fluorescence signals were mostly localized to the tumor, with only small amounts being observed in other tissues or organs.

Tumor-bearing mice were then euthanized and main organs along with glioma tissues were removed for determining the distribution of NPs in vivo at 72 hours post-drug administration. Fluorescence signals were present in tumor

tissues as well as the liver, spleen, lung, and kidney, while no signals were observed in other (nontumor) brain tissue sites (Figure 5B). Fluorescence intensity quantitative analysis of main organs is presented in Figure 5C. The level of fluorescence signals in tumor tissue was obviously higher than that in normal brain tissues.

Tumor MR imaging in vivo

In vivo MR imaging was performed in glioma-bearing rats on the 18th day after implantation. MR T_2-weighted images of rat brain were obtained before and after injection of multifunctional NPs. As shown in Figure 6A, glioma was characterized by hyper-intense signals in the T_2-weighted

MRI before the injection of SPIO@DSPE-PEG/DOX/ICG NPs. Both normal brain zones and glioma sites were darkened at 1 hour post-injection, with darkening of brain areas being more obvious than that at the tumor site. Negative contrast enhancements within the brain gradually diminished from 1 to 4 hours, and signal intensities at 4 hours post-injection were similar to those seen before injection. In contrast, negative contrast enhancements at the tumor site increased in strength from 1 to 24 hours. At 24 hours, the tumor site exhibited the most obvious decrease in T_2-weighted MR intensity as compared with the other time points. At 60 hours post-injection, negative contrasts at the tumor site remained enhanced as compared with other areas within the brain
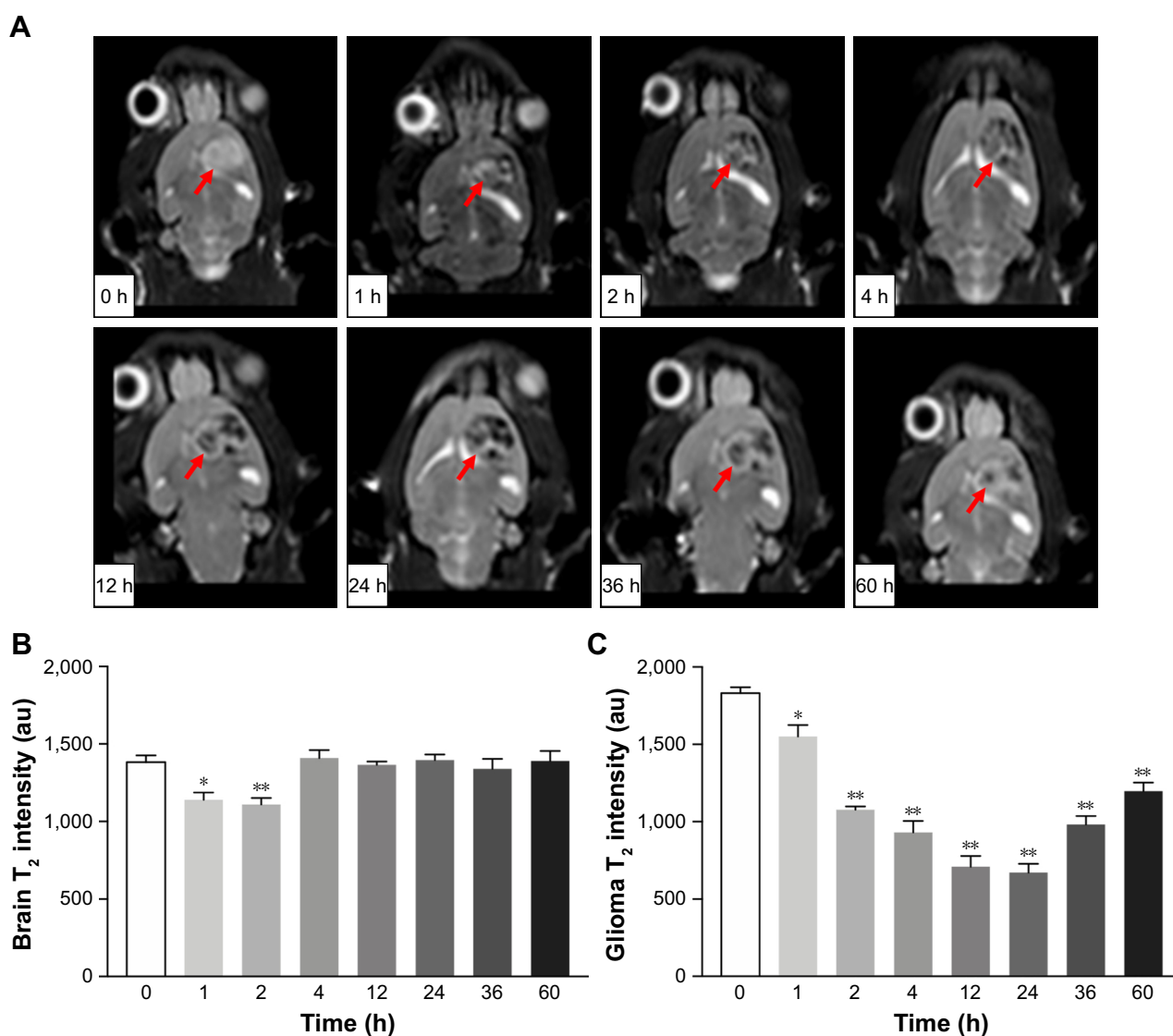

Figure 6 In vivo MRI efficacy.
Notes: T_2-weighted MR images of glioma-bearing Wistar rats at different times after tail vein injection of SPIO@DSPE-PEG/DOX/ICG NPs (**A**); arrow indicates direction of the glioma. The quantitative analyses of the T_2 value in brain (**B**) and tumor (**C**). Data are mean ± SD, n=3, *$P<0.05$ and **$P<0.01$ vs 0 hours.
Abbreviations: DOX, doxorubicin; DSPE-PEG, 1,2-distearoyl-sn-glycero-3-phosphoethanolamine-*N*-[methoxy(polyethylene glycol)]; ICG, indocyanine green; MRI, magnetic resonance imaging; SPIO NPs, superparamagnetic iron oxide nanoparticles.

indicating that the multifunctional NPs persisted in the tumor for at least 60 hours. The quantitative analyses of the T_2 values in brain and tumor are presented in Figure 6B and C, respectively. The T_2 value within the non-tumor areas of the brain decreased at 1–2 hours post-injection and was similar to that obtained before injection at 4 hours (Figure 6B). The T_2 value at the tumor site was significantly reduced from 1 to 60 hours after the injection and was most obvious at 24 hours (Figure 6C).

Antitumor efficiency and biocompatibility in vivo

To investigate the chemotherapeutic efficacy of SPIO@DSPE-PEG/DOX/ICG NPs in orthotopic glioma-bearing rats, tumor sizes were monitored in real time with use of MRI. T_1-weighted brain MR images were enhanced by gadolinium in a time-dependent manner as shown in Figure 7A. On the seventh day after implantation, similar tumor sizes were observed in all rats. A rapid enlargement in tumor size can be easily observed in brain MR images of rats treated with saline solution, SPIO@DSPE-PEG NPs, and free DOX, whereas rats treated with SPIO@DSPE-PEG/DOX/ICG

NPs displayed the slowest rates of tumor growth. With the exception of the SPIO@DSPE-PEG/DOX/ICG NPs group, extensive cerebral ventricle compression and a midline shift were observed in all other groups of rats. Based on MR images, the volumes of gliomas were calculated and shown in Figure 7B. Tumors in the control group of rats (saline) grew rapidly from 83.60 ± 12.23 mm³ on day 7 to 635.41 ± 47.65 mm³ on day 21. Similar results were obtained in rats treated with SPIO@DSPE-PEG NPs where tumors grew from 84.00 ± 11.02 mm³ to 640.11 ± 51.98 mm³ ($P>0.05$ vs control group), indicating that SPIO@DSPE-PEG NPs exhibited no obvious suppression of these glioma tumors. Tumors in rats treated with free DOX grew from 83.39 ± 11.95 mm³ to 270.25 ± 30.53 mm³ from days 7 to 21 ($P<0.001$ vs control group). Most significantly, tumor growth was essentially absent in rats treated with SPIO@DSPE-PEG/DOX/ICG NPs. In this group, tumor size was 83.62 ± 12.79 mm³ on day 7 and 110.02 ± 23.23 mm³ on day 21 ($P<0.001$ vs all groups), which demonstrates a complete inhibition of glioma growth in response to SPIO@DSPE-PEG/DOX/ICG NPs.

The therapeutic benefits of any cancer treatment are mainly indicated by improving the patient's quality of
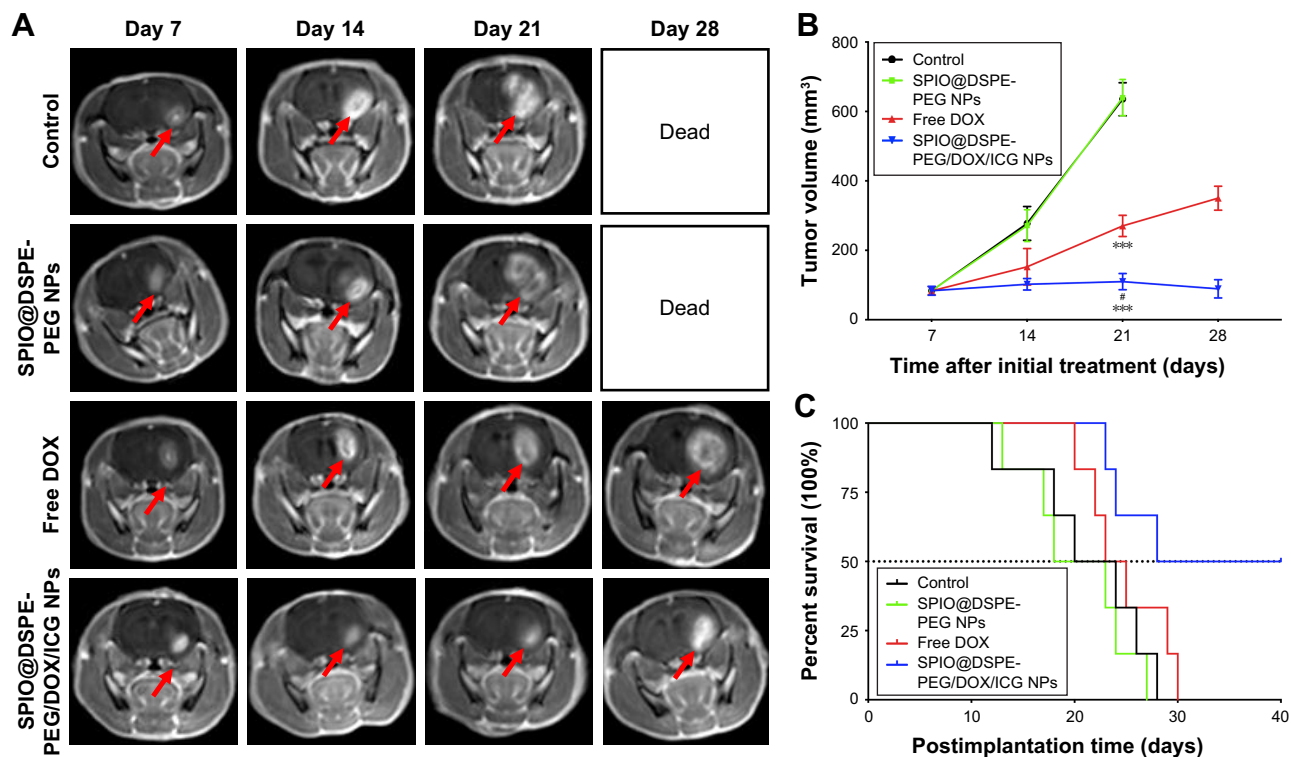

Figure 7 Antitumor efficacy in vivo.
Notes: T_1-weighted brain MR images of glioma-bearing Wistar rats treated with saline, SPIO@DSPE-PEG NPs, free DOX, and SPIO@DSPE-PEG/DOX/ICG NPs on days 7, 14, 21, and 28 after tumor implantation (**A**); arrow indicates direction of the glioma. Tumor volumes monitored by MRI (**B**). Kaplane–Meier survival curves (**C**) of rats. Data are shown as mean ± SD, n=6. ***$P<0.001$ vs control group, #$P<0.001$ vs free DOX group.
Abbreviations: DOX, doxorubicin; DSPE-PEG, 1,2-distearoyl-sn-glycero-3-phosphoethanolamine-N-[methoxy(polyethylene glycol)]; ICG, indocyanine green; MR, magnetic resonance; SPIO NPs, superparamagnetic iron oxide nanoparticles.
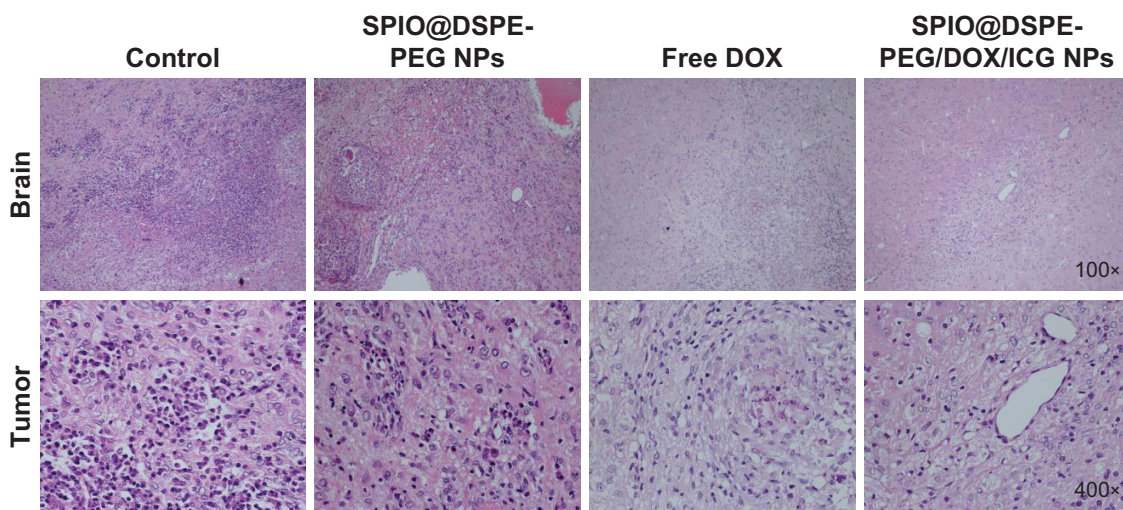
Figure 8 Histological sections of brain and tumor stained with H&E.
Abbreviations: DOX, doxorubicin; DSPE-PEG, 1,2-distearoyl-sn-glycero-3-phosphoethanolamine-N-[methoxy(polyethylene glycol)]; ICG, indocyanine green; SPIO NPs, superparamagnetic iron oxide nanoparticles.

life and prolonging their survival time. Survival and body weights of rats receiving the different treatments of this experiment were monitored after implantation and are presented in Figures 7C and S1. The control group exhibited relatively short survival times and a rapid loss in body weight. The SPIO@DSPE-PEG NP group showed similar responses in these two parameters as those observed in the control group. In contrast, both the free DOX and SPIO@DSPE-PEG/DOX/ICG NP groups showed more prolonged survival times and diminished losses in body weights. Notably, maximal survival times and slowest losses in body weights were obtained with the SPIO@DSPE-PEG/DOX/ICG NP group.

Histology and apoptpsis analysis

H&E staining and TUNEL assay were performed to further evaluate the therapeutic effects among these groups. H&E-stained sections of the control and SPIO@DSPE-PEG NP groups displayed significant nuclear polymorphism and plasmocyte infiltration (Figure 8). Sections obtained from the SPIO@DSPE-PEG/DOX/ICG NP group showed dramatically increased rates of tumor apoptosis and necrosis as compared with the other three groups (Figures 8 and S2), further demonstrating the antitumor ability of these multifunctional nanoparticles.

To evaluate the safety, toxicity, and side effects of SPIO@DSPE-PEG/DOX/ICG NPs within glioma-bearing rats during the treatment, H&E-stained sections from the heart, liver, spleen, lung, kidney, and muscle were examined (Figure S3). No obvious toxic pathological changes were

observed in any of these sections, indicating that these multifunctional NPs exerted no significant toxicity in rats.

Discussion

The treatment of intracranial gliomas has been problematic for clinicians due to the invasive growth of glioma and absence of appropriate imaging methods. Moreover, the presence of the BBB seriously impedes the penetration of most traditional chemotherapeutic drugs into the brain.[10] All these factors greatly reduce the therapeutic effect of glioma. Nanocarriers have the capacity to deliver a number of chemotherapy drugs as well as a variety of imaging contrast agents across the BBB and enable them to accumulate at the tumor site.[12,13] So, in this study we constructed a novel nanotheranostic agent which integrates bimodal imaging and chemotherapy to result in a significant improvement in the treatment of glioma.

The obtained SPIO@DSPE-PEG/DOX/ICG NPs possessed an average diameter of 22.9 nm. The small size of the NP could enhance its capacity for uptake within tumor cells while decreasing the uptake by macrophages,[32] which then contributes to its efficacy of treatment and avoids clearance by the reticuloendothelial system (RES). It has been reported previously that nanospheres are readily internalized by tumor cells, which would result in an improvement of their treatment effect.[33] Zeta potential is an important index to characterize the surface charge of NPs. This parameter is closely related to the stability of the NP, and the zeta potential is often used to predict and control stability of the colloidal system.[34] The amount of surface charge, approximately −38 mv, would

contribute to good stability due to electrostatic repulsion. After coating with DSPE-PEG 2000, hydrophobic DOX and amphiphilic ICG can be incorporated into the phospholipid layer outside the SPIO NP core by hydrophobic interaction. The encapsulating mass ratios of DOX to SPIO were 1:2 when the loading mass ratios of DOX to SPIO were 3:4, which is consistent with dosage levels of 5 and 10 mg/kg, respectively.[35,36] In this way, the dose administered can be limited to avoid excessive exposures upon other body systems. In addition to LC and EE, drug release characteristics also play a significant role in the application of the drug carrier. The NPs exhibited a slow and sustained drug release with a biphasic release pattern. The relatively fast initial release was probably due to the release of DOX adsorbed onto the NP surface, while the subsequent sustained release was most likely due to the enhanced membrane permeability of DOX encapsulated by DSPE-PEG2000. Such a release profile within tumor cells may enable a more effective drug delivery system to produce an enhanced chemotherapeutic outcome. It is well known that cellular internalization efficiency of drug carriers represents a major factor in their therapeutic efficacies. As shown in Figure 3, the fluorescence signal was mainly located within the cell nucleus, probably due to antitumor effects of DOX acting upon DNA.[37] An obvious fluorescence signal was observed in tumor cells treated with SPIO@DSPE-PEG/DOX/ICG NPs, which is likely a result of increased cellular uptake of DOX encapsulated in NPs via endocytosis. Lin et al also reported that cellular uptake of NPs could be improved significantly by a PEG modification.[38] Additionally, the blank NPs exhibited no obvious cytotoxicity for cells (Figure 4A). Therefore, SPIO@DSPE-PEG NPs as a carrier for DOX not only facilitated the delivery of DOX into cancer cells but also exhibited excellent biocompatibility, which suggests the potential for use of SPIO@DSPE-PEG/DOX/ICG NPs as a means for targeting drug delivery in the treatment of glioma.

Both in vivo near-infrared fluorescence imaging and MR imaging were utilized to investigate glioma targeting and imaging efficiency of the multifunctional NPs in an animal model of orthotopic glioma. As shown in Figure 5A, signals of free ICG were initially observed throughout the body at 2 hours post-injection, most likely representing that located within the skin, subcutaneous tissue, and viscera, such as the liver and intestinal tract.[39] The signals then showed a gradual time-dependent diminution with no intense signals being localized to the tumor site, indicating that free ICG molecules cannot target and accumulate at the tumor site. In contrast, fluorescence signals of NPs were mostly localized to the tumor at 24 hours, consistent with results presented in Figure 6A. These results suggest that large amounts of SPIO@DSPE-PEG/DOX/ICG NPs effectively crossed the BBB and specifically accumulated within the tumor site, but not in other brain regions. This can be attributed to the enhanced permeation and retention effect of NPs,[40,41] which also enables them to contribute to their outstanding imaging efficacy and reductions in side effects associated with chemotherapy for glioma. Moreover, with the introduction of the PEGylated phospholipid layer on the surface of SPIO, NPs avoid recognition by macrophages and thus removal by the RES of the liver and spleen.[42] This capacity results from their enhanced hydration property, which can then contribute to prolonged duration within the circulation. Intense fluorescence signals were observed in the liver and kidney, which indicated the main metabolic sites of the NPs. Fluorescence signals were also observed in the spleen and lung, probably due to the capture of RES within the spleen and the uptake of pulmonary endothelial cells, which can also act as a clearance pathway.[43]

The SPIO@DSPE-PEG/DOX/ICG NPs exhibited lower in vitro antitumor effect than that of free DOX after 24 and 48 hours of incubation periods (Figure 4B and C). This results from an increased amount of the drug in the free DOX group being in direct contact with the tumor cells, thus exerting an antitumor effect, while only a limited amount of drug is released from the SPIO@DSPE-PEG/DOX/ICG NPs to destroy the tumor cells. After a 72-hour incubation period, the NPs exhibited similar levels of cytotoxicity to that observed for free DOX at concentrations of 5 and 10 μg/mL. The results obtained at this time period indicate that SPIO@DSPE-PEG/DOX/ICG NPs greatly improved their efficacy as an antitumor drug. As a result, these low doses of DOX-loaded NPs now achieved the same efficacy as the free DOX drugs. In vivo SPIO@DSPE-PEG/DOX/ICG NP treatment resulted in a remarkable antitumor effect against glioma as compared with all other groups examined. Such advantageous effects might be attributed to the selective accumulation at tumor site, enhanced uptake by tumor cells, and sustained release of drug from NPs. Moreover, no obvious toxic pathological changes were observed in any of the organs as examined using H&E staining. These H&E staining results demonstrated an excellent degree of biocompatibility with the blank SPIO@DSPE-PEG NPs and no apparent side effects of SPIO@DSPE-PEG/DOX/ICG NP treatment.

Taken together, the multifunctional NPs, which integrate MR/fluorescence bimodal imaging and chemotherapy, was constructed for, and effective in, overcoming these obstacles.

This novel multifunctional NP has promising applications in the simultaneous improvement of surgical and chemotherapeutic outcomes. Our future work will be directed at modifying NPs with actively targeted bioactive ligands to further improve their theranostic effect.

Conclusion

A multifunctional nanotheranostic agent was successfully constructed by simultaneously loading DOX and ICG into the DSPE-PEG 2000 coated SPIO NPs for MR/fluorescence dual-modal imaging and chemotherapy of glioma. The NPs were of an appropriate size to enable a sustained release of drugs, an effective cellular uptake of DOX, and enhanced cytotoxicity effects directed against glioma cells as compared with that of a free DOX administration. Furthermore, the NPs possessed outstanding imaging capacities, penetration of the BBB, and the ability to show a discriminatory accumulation within the tumor site. As a result of these properties, this multifunctional NP exhibited the highest antitumor efficacy against C6 glioma-bearing rats and showed the fewest number of side effects. Collating results from these experiments, our findings demonstrate the efficacy of this multifunctional NP for the theranostic treatment of glioma.

Acknowledgments

Disclosure

The authors report no conflicts of interest in this work.

References

1. Ricard D, Idbaih A, Ducray F, Lahutte M, Hoang-Xuan K, Delattre JY. Primary brain tumours in adults. *Lancet*. 2012;379(9830):1984–1996.
2. Wen PY, Kesari S. Malignant gliomas in adults. *N Engl J Med*. 2008; 359(5):492–507.
3. Yang I, Aghi MK. New advances that enable identification of glioblastoma recurrence. *Nat Rev Clin Oncol*. 2009;6(11):648–657.
4. Anton K, Baehring JM, Mayer T. Glioblastoma multiforme: overview of current treatment and future perspectives. *Hematol Oncol Clin North Am*. 2012;26(4):825–853.
5. Weller M, Cloughesy T, Perry JR, Wick W. Standards of care for treatment of recurrent glioblastoma – are we there yet? *Neuro Oncol*. 2013; 15(1):4–27.
6. Senft C, Bink A, Franz K, Vatter H, Gasser T, Seifert V. Intraoperative MRI guidance and extent of resection in glioma surgery: a randomised, controlled trial. *Lancet Oncol*. 2011;12(11):997–1003.
7. Stummer W, Pichlmeier U, Meinel T, et al. Fluorescence-guided surgery with 5-aminolevulinic acid for resection of malignant glioma: a randomised controlled multicentre phase III trial. *Lancet Oncol*. 2006; 7(5):392–401.

8. Liu H, Zhang J, Chen X, et al. Application of iron oxide nanoparticles in glioma imaging and therapy: from bench to bedside. *Nanoscale*. 2016;8(15):7808–7826.
9. Frangioni JV. In vivo near-infrared fluorescence imaging. *Curr Opin Chem Biol*. 2003;7(5):626–634.
10. Bhujbal SV, de Vos P, Niclou SP. Drug and cell encapsulation: alternative delivery options for the treatment of malignant brain tumors. *Adv Drug Deliv Rev*. 2014;67–68:142–153.
11. Yang ZZ, Li JQ, Wang ZZ, Dong DW, Qi XR. Tumor-targeting dual peptides-modified cationic liposomes for delivery of siRNA and docetaxel to gliomas. *Biomaterials*. 2014;35(19):5226–5239.
12. Zhang F, Lin YA, Kannan S, Kannan RM. Targeting specific cells in the brain with nanomedicines for CNS therapies. *J Control Rel*. 2016;240:212–226.
13. Wong HL, Wu XY, Bendayan R. Nanotechnological advances for the delivery of CNS therapeutics. *Adv Drug Deliv Rev*. 2012;64(7):686–700.
14. Sharifi S, Behzadi S, Laurent S, Forrest ML, Stroeve P, Mahmoudi M. Toxicity of nanomaterials. *Chem Soc Rev*. 2012;41(6):2323–2343.
15. Na Hb, Song IC, Hyeon T. Inorganic Nanoparticles for MRI Contrast Agents. *Adv Mater*. 2009;21(21):2133–2148.
16. Zhang Y, Kohler N, Zhang M. Surface modification of superparamagnetic magnetite nanoparticles and their intracellular uptake. *Biomaterials*. 2002;23(7):1553–1561.
17. Veiseh O, Sun C, Gunn J, et al. Optical and MRI multifunctional nanoprobe for targeting gliomas. *Nano Lett*. 2005;5(6):1003–1008.
18. Hollins B, Noe B, Henderson JM. Fluorometric determination of indocyanine green in plasma. *Clin Chem*. 1987;33(6):765–768.
19. Cai W, Gao H, Chu C, et al. Engineering Phototheranostic Nanoscale Metal-Organic Frameworks for Multimodal Imaging-Guided Cancer Therapy. *ACS Appl Mater Interfaces*. 2017;9(3):2040–2051.
20. Zhou J, Yang F, Jiang G, Wang J. Applications of indocyanine green based near-infrared fluorescence imaging in thoracic surgery. *J Thorac Dis*. 2016;8(Suppl 9):S738–S743.
21. Stanga PE, Lim JI, Hamilton P. Indocyanine green angiography in chorioretinal diseases: indications and interpretation: an evidence-based update. *Ophthalmology*. 2003;110(1):15–21.
22. Reuthebuch O, Haussler A, Genoni M, et al. Novadaq SPY: intraoperative quality assessment in off-pump coronary artery bypass grafting. *Chest*. 2004;125(2):418–424.
23. Halle BM, Poulsen TD, Pedersen HP. Indocyanine green plasma disappearance rate as dynamic liver function test in critically ill patients. *Acta Anaesthesiol Scand*. 2014;58(10):1214–1219.
24. Raabe A, Beck J, Gerlach R, Zimmermann M, Seifert V. Near-infrared indocyanine green video angiography: a new method for intraoperative assessment of vascular flow. *Neurosurgery*. 2003;52:132–139.
25. Takagi Y, Kikuta K, Nozaki K, Sawamura K, Hashimoto N. Detection of a residual nidus by surgical microscope-integrated intraoperative near-infrared indocyanine green videoangiography in a child with a cerebral arteriovenous malformation. *J Neurosurg*. 2007;107(5 Suppl): 416–418.
26. Schubert GA, Schmieder K, Seiz-Rosenhagen M, Thomé C. ICG videography facilitates interpretation of vascular supply and anatomical landmarks in intramedullary spinal lesions: two case reports. *Spine*. 2011;36(12):E811–E813.
27. Gao C, Deng ZJ, Peng D, et al. Near-infrared dye-loaded magnetic nanoparticles as photoacoustic contrast agent for enhanced tumor imaging. *Cancer Biol Med*. 2016;13(3):349–359.
28. Lin J, Li Y, Li Y, et al. Drug/Dye-Loaded, Multifunctional PEG-Chitosan-Iron Oxide Nanocomposites for Methotraxate Synergistically Self-Targeted Cancer Therapy and Dual Model Imaging. *ACS Appl Mater Interfaces*. 2015;7(22):11908–11920.
29. Tong S, Hou S, Zheng Z, Zhou J, Bao G. Coating optimization of superparamagnetic iron oxide nanoparticles for high T2 relaxivity. *Nano Lett*. 2010;10(11):4607–4613.
30. Ma Y, Liang X, Tong S, Bao G, Ren Q, Dai Z. Gold Nanoshell Nanomicelles for Potential Magnetic Resonance Imaging, Light-Triggered Drug Release, and Photothermal Therapy. *Adv Funct Mater*. 2013;23(7): 815–822.

31. Ma Y, Tong S, Bao G, Gao C, Dai Z. Indocyanine green loaded SPIO nanoparticles with phospholipid-PEG coating for dual-modal imaging and photothermal therapy. *Biomaterials*. 2013;34(31):7706–7714.

32. Choi JS, Cao J, Naeem M, et al. Size-controlled biodegradable nanoparticles: preparation and size-dependent cellular uptake and tumor cell growth inhibition. *Colloids Surf B Biointerfaces*. 2014;122:545–551.

33. Zhang Y, Tekobo S, Tu Y, et al. Permission to enter cell by shape: nanodisk vs nanosphere. *ACS Appl Mater Interfaces*. 2012;4(8):4099–4105.

34. Heurtault B, Saulnier P, Pech B, Proust JE, Benoit JP. Physico-chemical stability of colloidal lipid particles. *Biomaterials*. 2003;24(23):4283–4300.

35. Jin X, Zou B, Luo L, et al. Codelivery of thioridazine and doxorubicin using nanoparticles for effective breast cancer therapy. *Int J Nanomed*. 2016;11:4545–4552.

36. Kim SG, Harel N, Jin T, Kim T, Lee P, Zhao F. Cerebral blood volume MRI with intravascular superparamagnetic iron oxide nanoparticles. *NMR Biomed*. 2013;26(8):949–962.

37. Yang F, Teves SS, Kemp CJ, Henikoff S. Doxorubicin, DNA torsion, and chromatin dynamics. *Biochim Biophys Acta*. 2014;1845(1):84–89.

38. Lin L, Wang X, Li X, et al. Modulating Drug Release Rate from Partially Silica-Coated Bicellar Nanodisc by Incorporating PEGylated Phospholipid. *Bioconjug Chem*. 2017;28(1):53–63.

39. Chen J, Liu C, Zeng G, et al. Indocyanine Green Loaded Reduced Graphene Oxide for In Vivo Photoacoustic/Fluorescence Dual-Modality Tumor Imaging. *Nanoscale Res Lett*. 2016;11(1):85.

40. Matsumura Y, Maeda H. A new concept for macromolecular therapeutics in cancer chemotherapy: mechanism of tumoritropic accumulation of proteins and the antitumor agent smancs. *Cancer Res*. 1986;46:6387–6392.

41. Velasco-Aguirre C, Morales F, Gallardo-Toledo E, et al. Peptides and proteins used to enhance gold nanoparticle delivery to the brain: preclinical approaches. *Int J Nanomed*. 2015;10:4919–4936.

42. Banerjee SS, Aher N, Patil R, Khandare J. Poly(ethylene glycol)-Prodrug Conjugates: Concept, Design, and Applications. *J Drug Deliv*. 2012;2012:103973.

43. Zhao P, Zheng M, Yue C, et al. Improving drug accumulation and photothermal efficacy in tumor depending on size of ICG loaded lipid-polymer nanoparticles. *Biomaterials*. 2014;35(23):6037–6046.
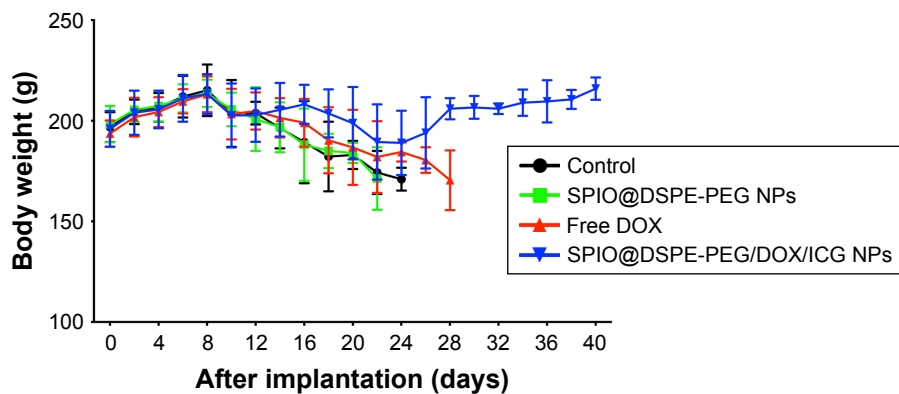
Supplementary materials

Figure S1 Body weights of glioma-bearing Wistar rats treated with saline, SPIO@DSPE-PEG NPs, free DOX, and SPIO@DSPE-PEG/DOX/ICG NPs. Data are shown as mean ± SD, n=6.
Abbreviations: DOX, doxorubicin; DSPE-PEG, 1,2-distearoyl-sn-glycero-3-phosphoethanolamine-N-[methoxy(polyethylene glycol)]; ICG, indocyanine green; SPIO NPs, superparamagnetic iron oxide nanoparticles.
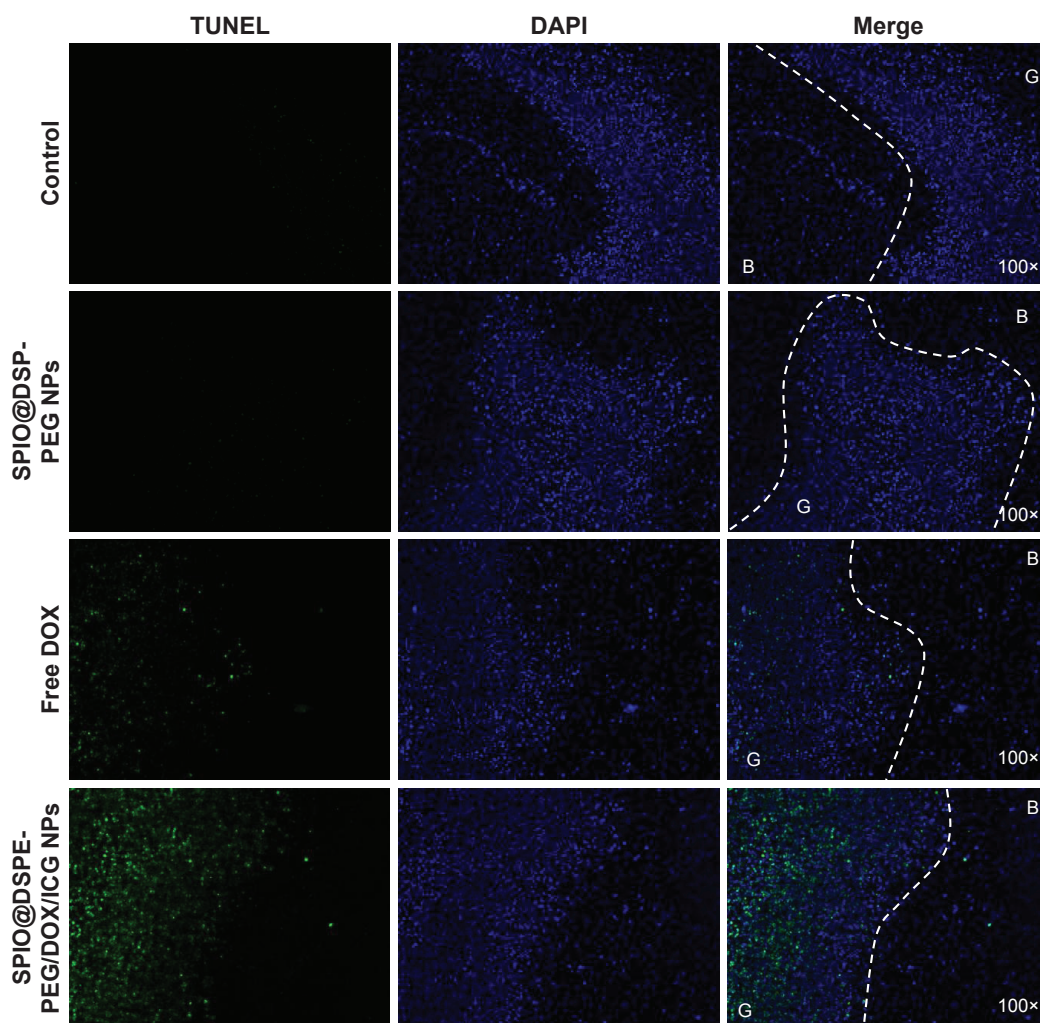

Figure S2 TUNEL analysis of frozen tumor sections after different treatments.
Note: Green: TUNEL-stained apoptosis cells; blue: DAPI-labeled cell nuclei; G: glioma tissues; B: brain tissues.
Abbreviations: DOX, doxorubicin; DSPE-PEG, 1,2-distearoyl-sn-glycero-3-phosphoethanolamine-N-[methoxy(polyethylene glycol)]; ICG, indocyanine green; SPIO NPs, superparamagnetic iron oxide nanoparticles.
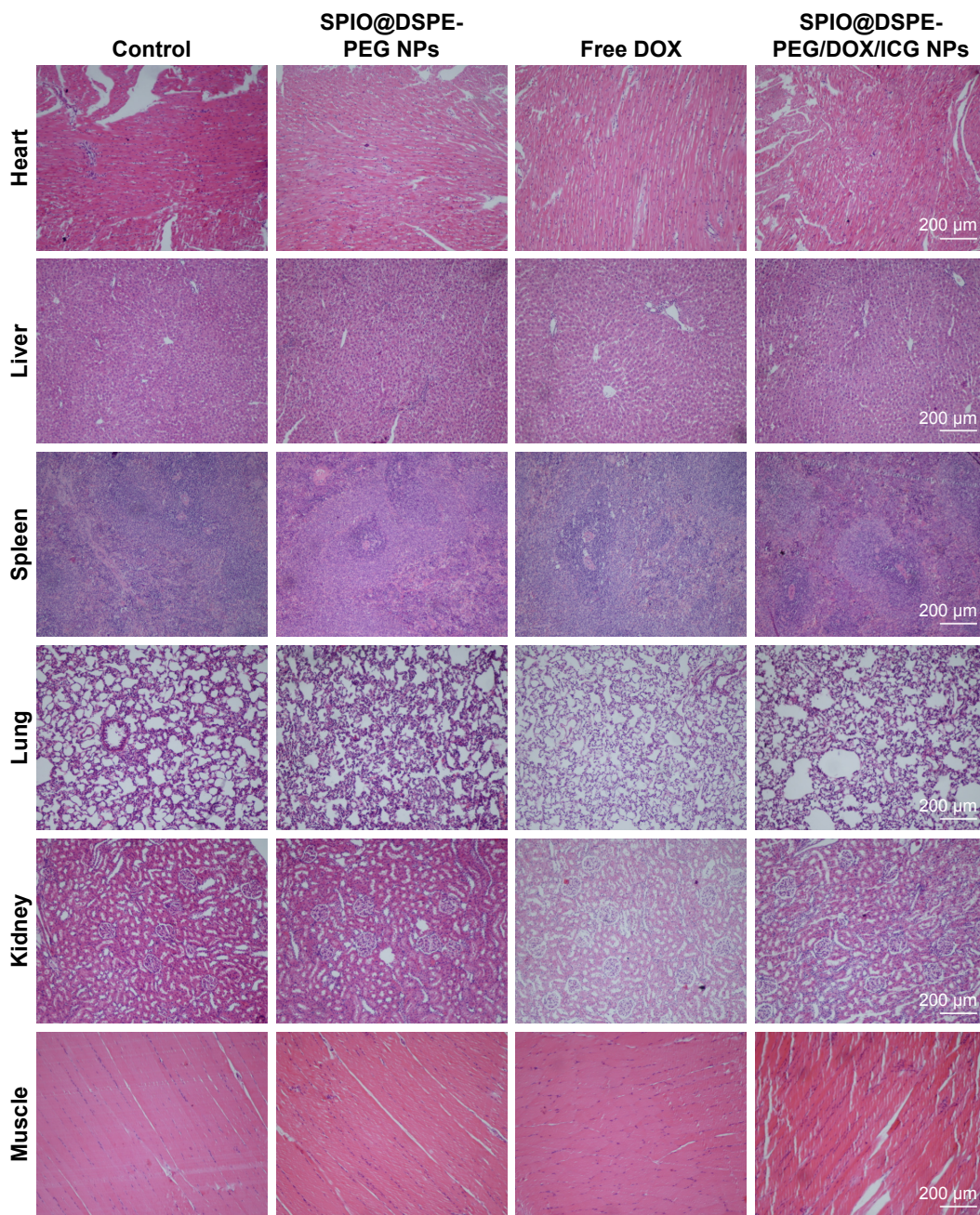
Figure S3 Histological sections of the heart, liver, spleen, lung, kidney, and muscle stained with H&E.
Abbreviations: DOX, doxorubicin; DSPE-PEG, 1,2-distearoyl-sn-glycero-3-phosphoethanolamine-N-[methoxy(polyethylene glycol)]; ICG, indocyanine green; SPIO NPs, superparamagnetic iron oxide nanoparticles.